Transversal convection patterns in horizontal shear flow

H. W. Müller and M. Lücke
Institut für Theoretische Physik, Universität des Saarlandes, D-6600 Saarbrücken, Federal Republic of Germany

M. Kamps
Forschungszentrum Jülich, Stabsstelle Supercomputing, D-5170 Jülich, Federal Republic of Germany
(Received 16 October 1991)

We investigate the influence of a horizontal plane Poiseuille shear flow transversal to the convective roll chain of the Rayleigh-Bénard problem. Using a one-dimensional (1D) amplitude equation and a 2D numerical simulation of the basic field equations, we study how different boundary conditions at the inlet and outlet of the channel affect nonlinear convection. If convection is suppressed near the cell apertures, spatially localized traveling-wave states appear with a uniquely selected bulk wavelength. For convectively unstable parameters this pattern is pushed out of the channel; however, the system becomes very sensitive to perturbations, and noise-driven structures occur. Phase-pinning boundary conditions lead for very small flows to stationary roll patterns with a space-dependent wavelength decreasing downstream. Strengthening the throughflow causes local Eckhaus instabilities, which finally generate a transition to propagating rolls.

PACS number(s): 47.20.Bp, 47.20.Ky, 47.60.+i

I. INTRODUCTION

The investigation of heated shear flows has a long history dating back to the 1920s [1]. The original motivation was geophysical problems like the formation of cloud streets, sand dunes, or oceanic mountains. Today this problem reobtains actuality due to its technical application in the fabrication of microelectronics involving chemical vapor deposition [2]. From a fundamental point of view the combination of the Rayleigh-Bénard problem [3] (thermal instability of a fluid layer heated from below) with the Orr-Sommerfeld problem [4] (instability of a shear flow) leads to an interesting nonlinear pattern-forming system. The basic conductive state is oscillatorily unstable with a frequency that is externally tunable by the strength of the imposed shear flow.

It has early been recognized [5] that convection in broad channels heated from below usually appears in the form of stationary rolls aligned parallel to the throughflow (longitudinal rolls). Traveling transversal rolls (axes perpendicular to the shear flow) have been detected [5,6] in narrow channels, but for small flow rates only. This is a result of two competing mechanisms: Perturbations in the form of longitudinal rolls are preferred by the throughflow, whereas transversal disturbances are favored by the influence of the lateral channel sidewalls [4,7]. From the theoretical point of view the properties of nonlinear convection in heated shear flows are hardly examined, so that the knowledge is mainly based on experiments [8–13] and two-dimensional numerical simulations [14–20] of the hydrodynamic field equations.

The majority of investigations is occupied with longitudinal convection patterns; only a few articles consider transversal roll structures. Luijkx, Platten, and Legros [11] reported transversal traveling roll patterns which did not fill the whole length of the channel. More recently, such spatially localized structures have been observed in numerical simulations [19,20]. They are a result [20] of the convective nature of the primary instability (which is a common feature of open flow systems like channel or pipe flows) and the absolute instability at higher Rayleigh numbers. Similar patterns also appear in the Taylor-Couette system with an axial throughflow [21,22]. In recent experimental work on Rayleigh-Bénard convection with throughflow competition between longitudinal and transversal rolls [13,23] has been observed; also a superposition of both structures and more complicated time-dependent behavior is possible. This competitive dynamics has been investigated by Brand, Ahlers, and Deissler [24] with a phenomenological model of two coupled amplitude equations for transversal and longitudinal rolls which, however, differ from the more rigorously derived equations [25].

Another kind of transversal convection structure has been studied by Pocheau *et al.* [26]. They used an annular conduit cell with azimuthally opposite flows in the two halves of the container. Due to this special geometry phase pinning occurs at the cell apertures and the system responds for small throughflow with a stationary deformed roll structure.

In the present work we consider transversal convective structures. In particular we address the question: How do the boundary conditions (BC) at the inlet and outlet of the channel affect the nonlinear convection? A short summary of our results has been published earlier [20]. Our investigation is based on two-dimensional (2D) computer simulations of the governing field equations as well as a 1D amplitude equation. After describing the system in Sec. II we present linear stability results in Sec. III and Appendix A. The amplitude equation, its important

properties, and derivation can be found in Sec. IV and Appendix B. Section V discusses different kinds of BC's at the entrance and exit of the container: Lateral periodic BC's are used to simulate a channel of infinite streamwise extension. A finite container is investigated with the aid of convection suppressing BC's; the influence of perturbations at the entrance is also studied. Phase-pinning BC's cause stationary deformed patterns as in the experiments of Pocheau *et al.* [26]. They are understood in terms of an inhomogeneous phase diffusion equation. For each type of boundary condition the outcomes of the amplitude equation are directly compared with numerical simulations of the hydrodynamic field equations. Wherever possible we discuss related experiments. Section VI gives a summary of our results.

II. THE SYSTEM

We consider a horizontal layer of an incompressible Boussinesq fluid between two rigid perfectly heat conducting plates at $z=0$ and 1. The fluid is heated from below and a lateral pressure gradient drives the throughflow in x direction. In the absence of lateral boundaries the basic conductive state is described by a linear temperature profile

$$T_{\text{cond}}=T_0+\text{Ra}(1-z) \tag{2.1a}$$

and a plane Poiseuille velocity field

$$\mathbf{U}(z)=6\sigma\,\text{Re}z(1-z)\mathbf{e}_x\ . \tag{2.1b}$$

Here we scaled lengths by d, times by d^2/κ, and temperature by $\kappa\nu/(\alpha g d^3)$. The Rayleigh number

$$\text{Ra}=\alpha g d^3\Delta T/(\kappa\nu) \tag{2.2a}$$

is given in terms of thermal expansion coefficient α, gravitational constant g, layer thickness d, thermal diffusivity κ, kinematic viscosity ν, and the temperature difference between the plates ΔT. The second control parameter is the Reynolds number

$$\text{Re}=\bar{U}d/\nu \tag{2.2b}$$

proportional to the vertically averaged flow velocity $\bar{U}$. After nondimensionalization one has $\bar{U}=\sigma\,\text{Re}$ where the Prandtl number $\sigma=\nu/\kappa$ is a material parameter of the fluid.

In a laterally unbounded layer linear stability analysis predicts [27] longitudinal convection rolls to grow first above threshold. However, in ducts with a small aspect ratio in y direction sidewall forcing dominates [28,29] and makes transversal rolls appear [4,7] provided the flow rate Re is below a certain threshold. To avoid the mathematical difficulties of a full three-dimensional analysis we are considering here an idealized situation where channel sidewalls indeed are necessary to enforce transversal rolls but where a two-dimensional description in the x-z plane perpendicular to the roll axes is a sufficient approximation. Thus we neglect the y component of the velocity and take all hydrodynamic fields to depend on x,z,t only. Then the governing equations for the convective contributions of temperature θ and velocity $\mathbf{u}=(u,0,w)$ read

$$\begin{bmatrix} -\partial_t(\partial_x^2+\partial_z^2)+\sigma(\partial_x^2+\partial_z^2)^2-6\sigma\,\text{Re}[2+z(1-z)(\partial_x^2+\partial_z^2)]\partial_x & \sigma\partial_x^2 \\ \text{Ra} & -\partial_t+(\partial_x^2+\partial_z^2)-6\sigma\,\text{Re}z(1-z)\partial_x \end{bmatrix}\begin{bmatrix} w \\ \theta \end{bmatrix} = \begin{bmatrix} \partial_x[u(\partial_x^2+\partial_z^2)w-w(\partial_x^2+\partial_z^2)u] \\ (u\partial_x+w\partial_z)\theta \end{bmatrix}. \tag{2.3a}$$

The continuity equation in the form

$$\partial_x u+\partial_z w=0 \tag{2.3b}$$

reflects incompressibility of the fluid. The operator on the left-hand side of (2.3) governs linear stability; all nonlinear terms are collected on the right-hand side.

III. LINEAR STABILITY

Due to the explicit z dependence of the left-hand side of (2.3) the stability problem is not analytically treatable so that we solved it numerically by a shooting algorithm. From earlier analysis it is known [27] that lateral throughflow stabilizes the basic conductive state against perturbations in the form of transversal rolls. In the following section we present how the dependences of the critical quantities can be expanded analytically for a small throughflow rate Re. Details of this computation are given in Appendix A. Note that the throughflow term in (2.3) breaks the x-reflection symmetry of the system. Only under simultaneous reversal of the flow direction ($\text{Re}\to-\text{Re}$) is the $x\to-x$ symmetry conserved. Consequently the critical Rayleigh number Ra_c as well as the critical wave number k_c are even functions of the Reynolds number, whereas the oscillation frequency ω_c is an odd one. In Appendix A we derive

$$\epsilon_c(\sigma,\text{Re})=\frac{1.262+1.392\sigma+128.5\sigma^2+21.26\sigma^3+24.59\sigma^4}{(\sigma+0.5117)^2}10^{-5}\text{Re}^2+O(\text{Re}^4)\ , \tag{3.1}$$

$$\omega_c(\sigma,\text{Re})=\sigma\frac{1.409+4.105\sigma}{\sigma+0.5117}\text{Re}+O(\text{Re}^3)\ , \tag{3.2}$$

where $\epsilon = \mathrm{Ra}/\mathrm{Ra}_c^0 - 1$ and $\mathrm{Ra}_c^0 = 1707.76$ is the critical Rayleigh number without flow. We do not give here the expression for $k_c(\sigma, \mathrm{Re})$ since it is rather unwieldy. Another consequence of the $\{x \to -x | \mathrm{Re} \to -\mathrm{Re}\}$ symmetry is that only *one* complex growth exponent belongs to a perturbation of given wave number k and not a *pair* of complex conjugate ones. Accordingly, the most general solution for the hydrodynamic fields $\phi = (u, w, \theta)$ close above threshold of stability is a traveling wave of the form

$$\phi(x,z,t) = A(x,t)\hat{\phi}(z)e^{i(k_c x - \omega_c t)} + \text{c.c.} \tag{3.3}$$

Here $\hat{\phi}(z) = (\hat{u}(z), \hat{w}(z), \hat{\theta}(z))$ is the complex eigenvector of the linear stability problem. For the small Reynolds numbers discussed here $\hat{\phi}(z)$ practically coincides with the (real) eigenfunctions of the Rayleigh-Bénard problem. The amplitude $A(x,t)$ governing the saturation and large-scale dynamics of the order parameter is undetermined in the framework of the linear analysis and will be discussed in the next section.

IV. AMPLITUDE EQUATION

In our system the bifurcation into the convective state is a forward oscillatory one. Thus in the vicinity of the bifurcation threshold the governing equation for the amplitude $A(x,t)$ is a Ginzburg-Landau equation with complex coefficients

$$\tau_0(\partial_t + v_g \partial_x)A = [\mu(1+ic_0) + \xi_0^2(1+ic_1)\partial_x^2 - \gamma(1+ic_2)|A|^2]A \ . \tag{4.1}$$

This equation results from a systematic expansion of (2.3) around the critical point $\epsilon_c(\mathrm{Re})$. The expansion parameter is $\sqrt{\mu}$, where

$$\mu = \frac{\mathrm{Ra}}{\mathrm{Ra}_c(\mathrm{Re})} - 1 = \frac{\epsilon - \epsilon_c(\mathrm{Re})}{1 + \epsilon_c(\mathrm{Re})} \tag{4.2}$$

measures the reduced distance between given Rayleigh number and actual threshold $\mathrm{Ra}_c(\mathrm{Re})$. The coefficients τ_0, ξ_0^2, and γ contain corrections $\sim \mathrm{Re}^2$ to their $\mathrm{Re}=0$ values. The group velocity v_g as well as the imaginary parts c_i are odd functions in Re, they grow in lowest order linearly with the flow rate. According to a work of Newell [30] the linear coefficients can be expressed by certain partial derivatives which we recall in Appendix B. For the coefficients γ and c_2 an extra nonlinear calculation is necessary. Details of this computation are also given in Appendix B. Of particular interest for our following discussion is the group velocity v_g. Its Re expansion turns out to be (see Appendix A)

$$v_g(\sigma, \mathrm{Re}) = \sigma \frac{0.3366 + 1.147\sigma + 1.325\sigma^2}{(\sigma + 0.5117)^2}\mathrm{Re} + O(\mathrm{Re}^3) \ . \tag{4.3}$$

In a realistic experimental situation, where the channel is of finite length, one has to deal with localized rather than extended perturbations. Applying the concept of absolute and convective instability [31] to Eq. (4.1) one finds that the basic conductive solution $A \equiv 0$ is convectively unstable if $\epsilon_c < \epsilon < \epsilon_c^{\mathrm{conv}}$ and absolutely unstable if $\epsilon > \epsilon_c^{\mathrm{conv}}$. The borderline between the two subregions is given by

$$\mu_c^{\mathrm{conv}} = \frac{\tau_0^2 v_g^2}{4\xi_0^2(1+c_1^2)} \ , \tag{4.4a}$$

$$\epsilon_c^{\mathrm{conv}} = \epsilon_c + (1+\epsilon_c)\mu_c^{\mathrm{conv}} \ . \tag{4.4b}$$

Obviously $\epsilon_c^{\mathrm{conv}} > \epsilon_c$ for finite throughflow. Using (3.1), (4.3), and the coefficients [32]

$$\tau_0 = \frac{\sigma + 0.5117}{19.65\sigma} + O(\mathrm{Re}^2) \ , \qquad \xi_0^2 = 0.148 + O(\mathrm{Re}^2), \quad c_1 = O(\mathrm{Re}) \tag{4.5}$$

we obtain

$$\epsilon_c^{\mathrm{conv}}(\sigma, \mathrm{Re}) = \frac{5.083 + 33.92\sigma + 109.4\sigma^2 + 135.1\sigma^3 + 79.3\sigma^4}{(\sigma + 0.5117)^2} 10^{-4}\mathrm{Re}^2 + O(\mathrm{Re}^4) \ . \tag{4.6}$$

In Fig. 1 we show $\epsilon_c^{\mathrm{conv}}$ and ϵ_c for a Prandtl number $\sigma = 1$.

If the control parameters ϵ and Re are such that the basic state $A \equiv 0$ is convectively unstable any *localized* initial disturbance is carried away by the throughflow so that rolls cannot grow globally. Leading and trailing edges of the perturbation propagate in the same direction, allowing the system behind the trailing front to return to its basic state. On the other hand, if the system is absolutely unstable any perturbation grows and expands everywhere (until nonlinear saturation), since leading and trailing fronts move in opposite directions. For $\mu > \mu_c^{\mathrm{conv}}$, or equivalently

$$v_f \equiv 2\frac{\xi_0}{\tau_0}[\mu(1+c_1^2)]^{1/2} > v_g \tag{4.7}$$

the speed v_f [33], with which the edges of a localized perturbation propagate in a *comoving frame* away from the center, is larger than the (downstream) center velocity v_g. Thus the velocity of the upstream facing front, $v_g - v_f$, is positive for $\mu < \mu_c^{\mathrm{conv}}$, negative for $\mu > \mu_c^{\mathrm{conv}}$, and zero at μ_c^{conv}.

V. NONLINEAR CONVECTION IN THE PRESENCE OF DIFFERENT BOUNDARY CONDITIONS

In this section we investigate how different kinds of boundary conditions at the inlet and outlet of the channel influence the nonlinear convective structure. We present results obtained by the amplitude equation (4.1) in direct

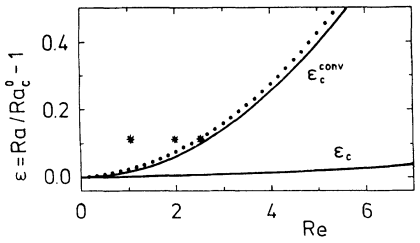

FIG. 1. The basic conductive state $A \equiv 0$ is stable below the threshold of linear stability ϵ_c, convectively unstable for $\epsilon_c < \epsilon < \epsilon_c^{conv}$, and absolutely unstable for $\epsilon > \epsilon_c^{conv}$. For convection suppressing inlet and outlet boundary conditions and in the absence of a continuous source of perturbations permanent convection is only possible in the absolutely unstable subregion. If $\epsilon_c^{conv}(\mathrm{Re})$ is approached from the left the streamwise growth length l of the roll pattern diverges. At the dotted line $l=10$. The stars indicate the control parameter combinations used for the simulations shown in Fig. 5.

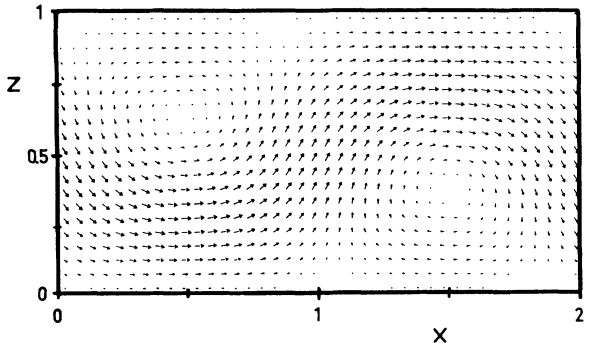

FIG. 2. Snapshot of the laterally periodic, fully developed velocity field for $\epsilon=0.114$, $\mathrm{Re}=1.67$. The arrows indicate local flow velocities in the x-z plane. The whole pattern moves downstream, to the right. Right (left) turning convection rolls are displaced downwards (upwards) due to the horizontal flow (2.1b).

comparison with two-dimensional computer simulations of the full hydrodynamic field equations. In doing so we use a finite difference formulation [34] which expresses spatial derivatives by central differences and applies a forward Euler step for the time integration. After each time step pressure and velocity fields are iteratively adapted to each other with the aid of a variant [35] of the SOLA code [36]. The spatial resolution was 20 grid points per unit length d, the temporal step size 5×10^{-4} time units (d^2/κ). We checked the accuracy of the algorithm by control runs with finer space and time resolution and found errors of less than 3% for velocity or temperature amplitudes; global quantities like the vertical heat transport through the layer are better approximated than 1%. All simulations have been performed with a Prandtl number of $\sigma=1$.

A. Periodic boundary conditions

The idealized case of a fluid layer which extends in streamwise direction to infinity is investigated by using periodic boundary conditions (i.e., inlet equals outlet). To drive the throughflow a pressure difference between entrance and exit of the channel was imposed, that is to say, ∇p was periodic. The periodicity length (the length of the channel) was $\Gamma=2$ keeping the wave number of the convection rolls fixed at $k=2\pi/\Gamma=\pi$, i.e., very close to the critical wave number $k_c(\mathrm{Re})=3.116+O(\mathrm{Re}^2)$.

Since periodic BC's do not allow initial perturbations to leave the channel the aforementioned distinction between absolute and convective instability is meaningless and *permanent* convection appears for *any* $\epsilon > \epsilon_c$. Figure 2 shows one periodicity length of the fully developed velocity field. The arrows indicate the local flow direction. Their lengths are proportional to the flow velocity. The whole pattern moves downstream (positive x direction) with a well-defined constant phase speed v_{phase}. Due to the horizontal velocity component of the basic Poiseuille flow right (left) turning convection rolls are displaced downwards (upwards). The vertical dependencies of the convective fields $\phi=(u,w,\theta)$ at an arbitrary x position agree well with the shape of the corresponding eigenfunctions $\hat{\phi}(z)$ predicted by the linear stability theory.

Under periodic BC's the long-time solution of the amplitude equation (4.1)

$$A(x,t)=A_0 e^{i[qx-\Omega(q)t]} \tag{5.1a}$$

describes a convective pattern of homogeneous amplitude

$$A_0=\sqrt{\mu/\gamma}(1-\xi_0^2 q^2/\mu)^{1/2}\ , \tag{5.1b}$$

uniform wave number $k=k_c+q$, and frequency $\omega=\omega_c+\Omega(q)$. The frequency correction is given by

$$\Omega(q)=\frac{1}{\tau_0}[\tau_0 v_g q+\xi_0^2 q^2(c_1-c_2)-\mu(c_0-c_2)]\ . \tag{5.1c}$$

Both amplitude A_0 as well as frequency shift Ω depend on the wave-number displacement q, which is a free parameter of the solution (5.1). To compare with our numerical solutions, where the wave number of the pattern is fixed at $k=\pi$, we have to impose $q=\pi-k_c$. Since k_c is very close to π in all of our runs, the correction factor $(1-\xi_0^2 q^2/\mu)^{1/2}$ in Eq. (5.1b) can be neglected in the following discussion.

An important quantity in convection experiments is the Nusselt number N, measuring the total vertical heat transfer through the layer reduced by its conductive contribution. In terms of the amplitude A it is given by

$$N=1+\frac{|A|^2}{1+\mu}=1+\frac{1}{\gamma}\frac{\mu}{1+\mu}\ , \tag{5.2}$$

where the second equality follows from Eqs. (5.1a) and (5.1b). Due to the weak Re dependence of the nonlinear coefficient γ (Appendix B) all simulation data for different Re are expected to collapse onto a common line, if they are plotted versus μ. This is confirmed by Fig. 3 where we compare our computer experiments with the analytic solution (5.2). The dotted line is a best fit through the simulation results (for $0\le\mu\lesssim0.5$ and $0<\mathrm{Re}\lesssim7$) with

$$N=1+1.423\frac{\mu}{1+\mu}(1+0.09\sqrt{\mu}) \ . \tag{5.3}$$

The leading term is in agreement with the amplitude equation result (5.2) where the calculation yields $1/\gamma=1.423+O(\mathrm{Re}^2)$ for $\sigma=1$ (see Appendix B).

The phase speed at which the whole roll pattern travels in flow direction is

$$v_{\mathrm{phase}}=\frac{\omega_c+\Omega(q)}{k_c+q}=\frac{\omega_c+v_g q+\xi_0^2 q^2(c_1-c_2)/\tau_0-\mu(c_0-c_2)/\tau_0}{\pi} \ . \tag{5.4}$$

Since ω_c, v_g, c_0, c_1, and c_2 are in lowest order proportional to Re it is useful to reduce v_{phase} by the mean throughflow velocity $\bar{U}=\sigma\,\mathrm{Re}$. Neglecting higher-order Re corrections the ratio $v_{\mathrm{phase}}/\bar{U}$ is independent of the flow rate and a function of Ra only. For $\sigma=1$ we obtain

$$\left.\frac{v_{\mathrm{phase}}}{\bar{U}}\right|_{\sigma=1}=1.171-0.0188\mu \ . \tag{5.5}$$

Figure 4 shows that this result agrees well with the simulation data. The systematic error of about 0.5% is a result of the discretization density in the finite difference algorithm; it reduces if the spatial and temporal resolution is improved. Equation (5.5) yields the theoretical explanation for the observation [18] that the pattern propagation velocity decreases linearly with the Rayleigh number if the flow rate Re is held fixed.

B. Convection suppressing boundary conditions

In this and the following Sec. V C we investigate more realistic convection channels with nonperiodic inlet and outlet boundary conditions. Since information is transported downstream by the shear flow the entrance BC turns out to be crucial for the convective behavior within the bulk. To study this problem we simulated convection in a channel of length $\Gamma=25$. In defining the boundary conditions we orient ourselves by the experiments published so far.

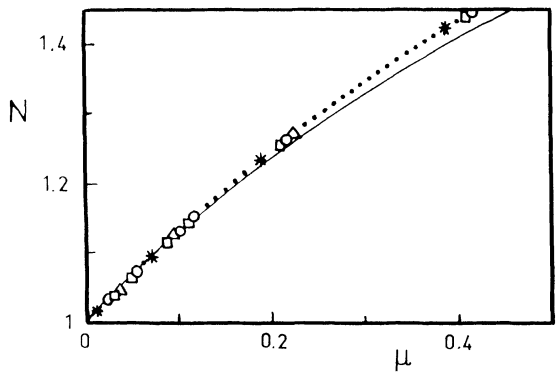

FIG. 3. The Nusselt number N as a function of the relative distance from threshold $\mu=\mathrm{Ra}/\mathrm{Ra}_c(\mathrm{Re})-1$. Solid line: Amplitude equation result according to (5.2); dotted line: best fit (5.3) through the simulation data for Re=0 (circles), 1.67 (triangles), 3.33 (squares), 6.67 (stars).

1. *Spatially confined convection patterns*

Luijkx, Platten, and Legros [11] used a porous plug at both ends of the duct to reduce inlet and outlet turbulence. Although there is no information about the velocity and temperature distribution near the porous walls it is reasonable to assume that convection is suppressed there. Accordingly in our simulations we enforced the basic field profiles $T_{\mathrm{cond}}(z)$ and $\mathbf{U}(z)$ (2.1) at the channel apertures at $x=0$ and $x=\Gamma$. Figure 5 presents snapshots of the vertical velocity field $w(x,z=0.5)$ after sufficient long integration time when a steady state has established. Thin lines are obtained from the numerical simulation of the full hydrodynamic equations. The thick envelope results from the final-state solution of the amplitude equation, which is of the form $A(x,t)=B(x)e^{i\omega t}$. The stationary envelope $|B(x)|$ increases over a distance $l(\mathrm{Re},\mathrm{Ra})$ to half its saturation value while the roll pattern propagates downstream. As observed in earlier simulations [19] the front of the envelope is pushed more and more downstream if the flow rate is increased. Note that the ϵ-Re control parameter combinations used in Fig. 5 (indicated by stars in Fig. 1) are within the absolutely unstable subregion. At $\epsilon_c^{\mathrm{conv}}(\mathrm{Re})$ the growth length l diverges. Entering into the convectively unstable region below the curve $\epsilon_c^{\mathrm{conv}}$ by increasing Re or decreasing ϵ any initial convection is "blown" completely out of the system.

We emphasize here the importance of the homogeneous (convection suppressing) inlet boundary condition which forbids new perturbations to penetrate into the cell. Permanent convection, therefore, is not possible for

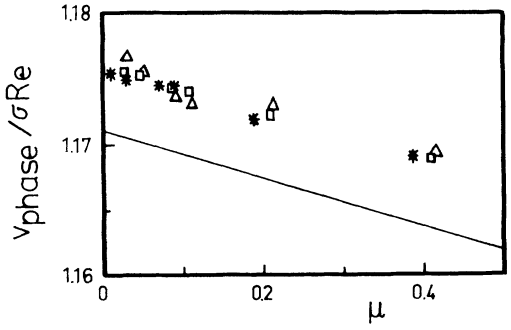

FIG. 4. The propagation velocity of the pattern v_{phase} reduced by the vertically averaged flow velocity $\bar{U}=\sigma\,\mathrm{Re}$. Solid line: amplitude equation result (5.5). Simulation data: Re=1.67 (triangles), 3.33 (squares), 6.67 (stars).

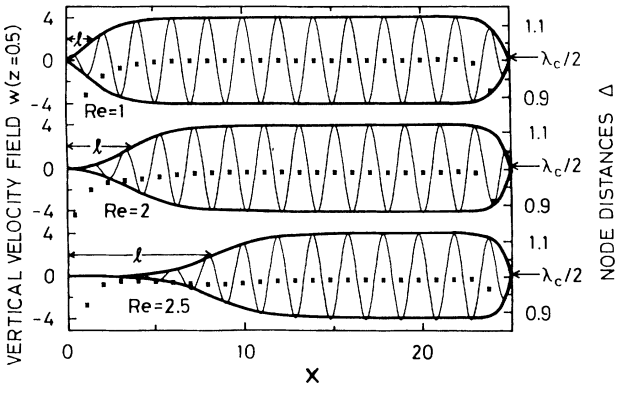

FIG. 5. Snapshots of the fully developed velocity field under convection suppressing inlet-outlet BC. The control parameters ($\epsilon=0.114$, Re as indicated) are such that the conductive state is absolutely unstable (cf. stars in Fig. 1). Thin lines show the vertical velocity field $w(x,z=0.5)$ taken from computer simulations of the full hydrodynamic equations. Local node distances $\Delta(x)$ (squares) are smaller than half the critical wavelength λ_c. The structures propagate to the right (downstream) the envelopes are stationary. Full lines are obtained by numerical solution of the amplitude equation (4.1) with $A=0$ at inlet-outlet. The envelopes grow from the inlet over a length l to half of the bulk value.

$\epsilon_c<\epsilon<\epsilon_c^{\rm conv}$ even though the basic conductive state is unstable to extended perturbations $\sim e^{ikx}$. Later we will demonstrate how a *continuous* source of disturbances (e.g., inlet turbulence) can change this behavior. Let us mention that the "blowing out" of the pattern is a reversible process: When crossing the borderline $\epsilon_c^{\rm conv}$ in Fig. 1 from below the propagating roll pattern invades the channel in upstream direction up to the appropriate distance $l(\mathrm{Re},\mathrm{Ra})$ from the inlet.

In Fig. 6 we compare l as computed from the amplitude equation (solid line) with the simulations of the full equations for various Re and Ra. With $L=\sqrt{\mu}l/\xi_0$ plotted versus $V_g(\mathrm{Re},\mathrm{Ra})=v_g\tau_0/[\xi_0^2\mu(1+c_1^2)]^{1/2}$ all simulation data fall onto the line resulting from the amplitude equation. This scaling behavior can be understood if the throughflow rate Re is small enough to neglect the imaginary parts c_0, c_1, and c_2 in the amplitude equation. With a stationary solution $\tilde{A}(x)=\sqrt{\gamma/\mu}A(x)$ and a rescaled space variable $X=\sqrt{\mu}x/\xi_0$ one finds from (4.1)

$$\partial_X^2\tilde{A}-V_g\partial_X\tilde{A}+\tilde{A}-\tilde{A}^3=0\ . \tag{5.6}$$

Since V_g is the only control parameter in this anharmonic oscillator equation it governs the reduced characteristic length L. The function $L(V_g)$ shown in Fig. 6 is universal in the sense that it is independent of the Prandtl number; all σ dependencies are contained in the scaling of the axis. The divergence condition $V_g=2$ is equivalent to $\epsilon=\epsilon_c^{\rm conv}$. The rapid increase of L close to $V_g=2$ is reflected in Fig. 1 by the dotted curve for $l=10$, which is very close to $\epsilon_c^{\rm conv}$ where the growth length l diverges. In the experiments of Luijkx, Platten, and Legros [11] and Ouazzani and Platten [37] propagating transversal roll patterns filled the whole channel for small flow rates whereas convection was more confined to the outlet region for increasing Reynolds numbers.

2. *Wavelength selection*

In our computer simulations we found a unique wavelength selection in the presence of throughflow. The solid squares in Fig. 5 indicate local distances between two adjacent rolls (which is half of the local wavelength). Characteristic spatial wavelength gradients appear in areas of strong amplitude variations while the convective bulk region shows a spatially uniform wavelength. For $\mathrm{Re}>0$ this selected bulk value turns out to be independent of the initial configuration and history of the system. It only depends on the final ϵ-Re combination and the Prandtl number σ. Also the length of the channel does not affect the selection mechanism. Obviously, the homogeneous convection suppressing BC's prevent phase pinning so that the traveling rolls are free to select their preferred wave number. Figure 7 demonstrates for $\sigma=1$ that the bulk wavelength λ weakly decreases with Re and Ra. This is in qualitative agreement with experiments [11] where the number of convection rolls was found to increase with growing flow rate. However the amplitude equation (4.1) with homogeneous $A=0$ inlet-outlet BC's

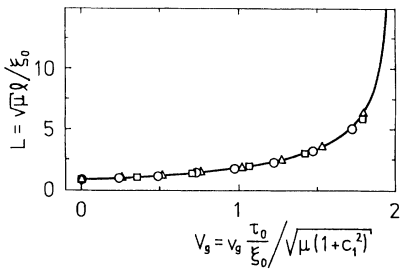

FIG. 6. Reduced growth length $L=\sqrt{\mu}l/\xi_0$ vs scaled group velocity $V_g=\tau_0 v_g/[\xi_0^2\mu(1+c_1^2)]^{1/2}$. Symbols result from computer simulations of the hydrodynamic field equations: $\epsilon=0.114$, $\mathrm{Re}\le 2.5$ (circles); $\epsilon=0.215$, $\mathrm{Re}\le 3.4$ (squares); $\epsilon=0.417$, $\mathrm{Re}\le 4$ (triangles). The solid line is obtained by integration of the amplitude equation. Near the divergence a fit shows $L\simeq 2.31(2-V_g)^{-0.637}$.

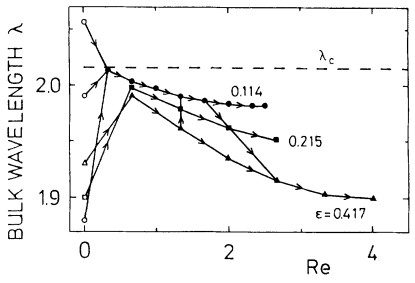

FIG. 7. Bulk wavelength selected in simulation runs: $\epsilon=0.114$ (circles), 0.215 (squares), 0.417 (triangles). In the presence of throughflow full symbols show the wavelengths selected independently of cell length and history of the system. Without throughflow ($\mathrm{Re}=0$) several stable states of different λ could be realized (open symbols), e.g., by varying the channel length. Arrows indicate simulation protocols.

does not reproduce these characteristic wavelength variations. There the selected values are always very close to the critical wavelength λ_c.

3. *Influence of perturbations*

Our foregoing discussion is based on the idealized assumption that the undisturbed basic conductive state is realized at the channel entrance. Experiments, however, always show a certain level of perturbations, e.g., inlet turbulence, other fluctuations, and thermal noise. Such a permanent source of disturbances turns out to be crucial if the system is convectively unstable.

To investigate this problem qualitatively we imposed in our simulations at the inlet a fluctuating vertical velocity field by using uncorrelated random numbers of vanishing mean. We performed runs with average noise amplitudes between 1% and 100% of the downstream convective saturation amplitude of w. For absolutely unstable ϵ-Re combinations the convection behavior was hardly affected by the inlet noise. Only in a short entrance region of a few roll diameters do stochastic variations of the envelope reflect the random inlet BC. With increasing distance from inlet the influence of the noise quickly decays and nonlinear convection behaves as in the undisturbed case.

For convectively unstable parameters the situation is completely different. Figure 8 shows the simulation results for $\epsilon=0.114$ and $\mathrm{Re}=3$. The phase of the pattern fluctuates and also the intensity envelope of the propagating rolls is no longer stationary but varies slightly around a mean profile. The temporal average of the growth length l is a monotonously decreasing function of the noise strength (*a*: 1%; *b*: 10%; *c*: 100%). Obviously, the system acts like a selective amplifier of the inlet disturbances with temporal and spatial delay. All convective structures are noise sustained [38], they die out as soon as the noise source is removed. This property might be a useful tool for quantitative measurements of the experimental noise. Note, even in the case of a *spatially extended* noise source disturbances originating close to the inlet would be amplified most since they have the longest downstream distances to grow.

The amplitude equation also shows this dynamics if the $A=0$ inlet BC is replaced by a noisy one. In the region close to the entrance, where the convective amplitude is still small, it follows from the linearized amplitude equation that a Fourier mode $A_0(\omega)$ of a noisy inlet amplitude $A_0(t)=A(x=0,t)$ increases downstream according to [38]

$$A(x,\omega)=A_0(\omega)e^{\kappa(\omega)x}$$

where

$$\kappa(\omega)=\frac{\tau_0 v_g}{2\xi_0^2(1+ic_1)}-\left[\left[\frac{\tau_0 v_g}{2\xi_0^2(1+ic_1)}\right]^2-\frac{\mu(1+ic_0)-i\omega\tau_0}{\xi_0^2(1+ic_1)}\right]^{1/2}. \tag{5.7}$$

Here the negative sign in front of the square root (with positive real part) must be taken to obtain the correct spatial growth behavior in *downstream* direction. This is easy to see because the condition $\mathrm{Real}[\kappa]<0$ (spatial decay) must be fulfilled if the conductive state is absolutely stable ($\mu<0$). Taking the positive square root in (5.7) yields the spatial growth or decay exponent of a signal in *upstream* direction. Neglecting the small imaginary parts c_0, c_1 the maximum spatial growth exponent appears for $\omega=0$ with

$$\kappa_{\max}=\kappa(\omega=0)\simeq\frac{\tau_0 v_g}{2\xi_0^2}\left[\left[\frac{\tau_0 v_g}{2\xi_0^2}\right]^2-\frac{\mu}{\xi_0^2}\right]^{1/2}. \tag{5.8}$$

Thus the fastest growing mode, $\omega=0$ (corresponding to ω_c in the order parameter), is amplified exponentially downstream by a factor $e^{\kappa_{\max}x}$. This result is also in accordance with our finite difference simulations: The straight dashed line in Fig. 8 connects downstream positions of the same small field amplitude resulting from noise that increases linearly on a log scale from Fig. 8(a) to 8(c). At a given channel position $x>0$ the isolines $\kappa_{\max}x=\text{const}$, or equivalently

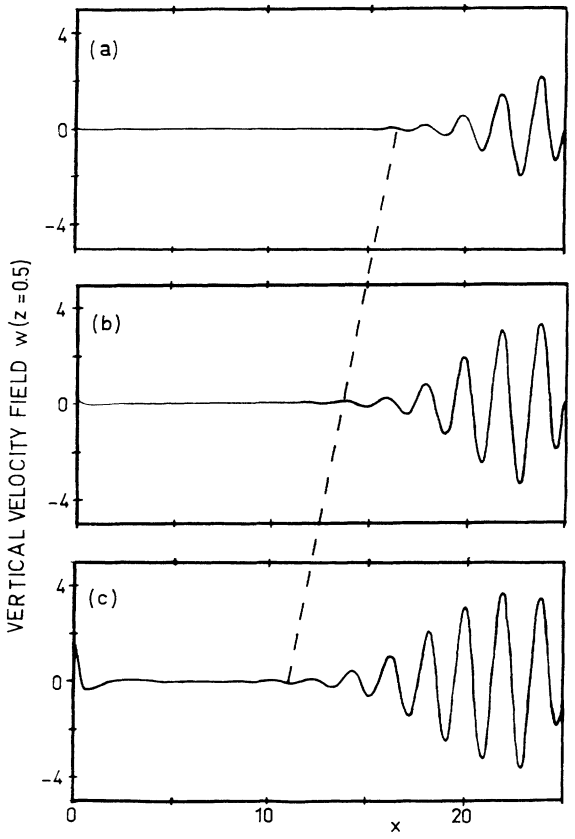

FIG. 8. Snapshots of the vertical velocity field $w(x,z=0.5)$ under the influence of inlet noise. Parameters, $\epsilon=0.114$ and $\mathrm{Re}=3$, are such that the basic conductive state is convectively unstable (cf. Fig. 1). The inlet noise amplitude of $w(x=0,z,t)$ is (a) 1%, (b) 10%, and (c) 100% of the saturation value of w. The whole pattern propagates downstream, the envelope fluctuates slightly around an (temporally) averaged distribution. If the inlet noise source is removed convection dies out. The straight dashed line connects downstream positions of the same small field amplitude.

$$\mu=\frac{\text{const}}{x}\tau_0 v_g-\left[\frac{\text{const}}{x}\right]^2\xi_0^2 , \tag{5.9}$$

define curves in the ϵ-Re control parameter plane where the same (small) convection amplitude occurs. We checked Eq. (5.9) with the experimental data and the coefficients of Babcock *et al.* (see their Fig. 6) and found good agreement for their three x positions with const$\simeq 6.2$. The foregoing "linear" argument only holds in the convectively unstable region. As soon as the system becomes absolutely unstable any perturbation expands in both horizontal directions and the form of the envelope is determined by the nonlinearity, so that no information can be obtained from Eqs. (5.7) and (5.8) for $\mu>\mu_c^{\text{conv}}$.

C. Phase-pinning boundary conditions

Instead of fixing the convective amplitude at inlet and outlet to be zero we now consider a phase-pinning BC. This investigation is motivated by experiments [26] with azimuthally opposite throughflow in the two halves of an annular conduit. In this situation a stationary deformed pattern appears for small Re while roll propagation sets in beyond a critical flow rate. To explain this dynamics phenomenological arguments have been used to extend the phase diffusion equation of the classical Rayleigh-Bénard problem by an additional advective term [26,39] to take the throughflow into account. In our following discussion we show how an equivalent phase equation can be rigorously deduced from the amplitude equation and compare its solutions with numerical simulations.

1. Derivation of the phase equation

To compensate the critical time dependence of the order parameter, $w\sim A(x,t)e^{-i\omega_c t}$, we introduce the amplitude

$$\tilde{A}(x,t)\equiv r(x,t)e^{i\psi(x,t)}=A(x,t)e^{-i\omega_c t} \tag{5.10}$$

and obtain from (4.1) the evolution equation

$$\tau_0(\partial_t+v_g\partial_x)\tilde{A}=\{[\mu(1+ic_0)-i\omega_c\tau_0]+\xi_0^2(1+ic_1)\partial_x^2 -\gamma(1+ic_2)|\tilde{A}|^2\}\tilde{A} . \tag{5.11}$$

Its stationary solution describes a stationary pattern. Since deformed patterns only occur for very small flow rates, we use an expansion in powers of Re:

$$\begin{aligned} r(x,t)&=r^{(0)}+r^{(1)}(x,t)\text{Re}+O(\text{Re}^2) ,\\ \psi(x,t)&=\psi^{(0)}(x)+\psi^{(1)}(x,t)\text{Re}+O(\text{Re}^2) \end{aligned} \tag{5.12}$$

to extract an equation of motion for the phase $\psi(x,t)$. In the absence of throughflow (Re$=0$) the coefficients v_g, c_0, c_1, c_2, and ω_c drop out and the lowest-order solution of (5.11)

$$r^{(0)}=\left[\frac{\epsilon-\xi_0^2q^2}{\gamma}\right]^{1/2}, \quad \psi^{(0)}(x)=qx \tag{5.13}$$

describes a stationary roll structure with an undisturbed uniform wave number $\bar{k}=k_c+q$. Here we used $\mu=\epsilon+O(\text{Re}^2)$.

In what follows we investigate how this basic convective structure is modified in the presence of a weak throughflow. From the imaginary part of (5.11) one finds in $O(\text{Re})$

$$\tau_0\partial_t\psi=\xi_0^2\partial_x^2\psi+2\xi_0^2q\frac{\partial_x r}{r^{(0)}} -\tau_0\left[\omega_c+v_g q+\frac{\xi_0^2}{\tau_0}q^2(c_1-c_2)-\frac{\epsilon}{\tau_0}(c_0-c_2)\right] . \tag{5.14}$$

After adiabatic elimination of the amplitude term $\partial_x r/r^{(0)}$ we obtain the following inhomogeneous phase diffusion equation:

$$\partial_t\psi=D_\parallel\partial_x^2\psi-(\omega_c+\Omega) \tag{5.15}$$

with the diffusion constant

$$D_\parallel=\frac{\xi_0^2}{\tau_0}\left[\frac{\epsilon-3\xi_0^2q^2}{\epsilon-\xi_0^2q^2}\right] . \tag{5.16}$$

The inhomogeneity

$$(\omega_c+\Omega)=\omega_c+v_g q+\frac{\xi_0^2}{\tau_0}q^2(c_1-c_2)-\frac{\epsilon}{\tau_0}(c_0-c_2) \tag{5.17}$$

increases in lowest order linearly with the flow rate. Note that the phase dynamics depends via $D_\parallel$ and Ω on the wave number $\bar{k}=k_c+q$ of the undisturbed roll structure. The stationary solution of (5.15)

$$\psi(x)=\frac{1}{2}\frac{\omega_c+\Omega}{D_\parallel}(x-\Gamma)x+qx \tag{5.18}$$

represents a standing deformed roll pattern with a local wave number

$$k(x)=k_c+\frac{\partial\psi}{\partial x}=k_c+q+\frac{\omega_c+\Omega}{D_\parallel}\left[x-\frac{\Gamma}{2}\right] \tag{5.19}$$

increasing linearly with a gradient $(\omega_c+\Omega)/D_\parallel$ proportional to Re. The integration constant in (5.19) was chosen such that the undisturbed wave number $\bar{k}=k_c+q$ occurs at $x=\Gamma/2$ in the middle between inlet and outlet as in the experiments [26]. Thus the largest deviations of $k(x)$ from $\bar{k}$ are located near the apertures of the conduit.

2. Comparison with simulation results

To incorporate phase fixing into our computer simulations we used as inlet-outlet boundary conditions

$$\partial_x w=\partial_x T=0 \quad \text{at } x=0 \text{ and } x=\Gamma$$

to pin maximal convective upflow or downflow at the apertures. The throughflow was increased step by step keeping $\epsilon=0.215$ constant. The time interval between two steps in Re was sufficiently long for the pattern to re-

lax to the new steady structure. The initial pattern at Re=0 consisted of 27 convection rolls of uniform wave number $\bar{k}=27\pi/\Gamma=3.393$. This value differs from $k_c=3.116$, the center of the stable Eckhaus band, by $q=\bar{k}-k_c=0.277$.

After switching on the throughflow to Re=0.0083 the whole structure relaxes to a new stationary deformed state whose final wave-number distribution is shown by the solid squares in Fig. 9. Near outlet, where the difference between $k(x)$ and k_c is largest the distribution becomes slightly nonlinear. In this region the pattern is less stiff because the diffusion constant $D_\parallel(q)$ is locally smaller there. This effect is not properly described by the solution of the phase equation (5.19) (solid line in Fig. 9) which assumes a uniform value for $D_\parallel$. However, direct integration of the amplitude equation (5.11) with phase fixing boundaries, $\psi=$const, at inlet-outlet correctly reproduces the nonlinear spatial wave-number profile. Further increase of Re steepens the wave-number profile (dashed line in Fig. 9) and induces a local instability near the outlet of the channel as soon as the upper Eckhaus threshold $k_E^+=k_c+[\epsilon/(3\xi_0^2)]^{1/2}$ is exceeded. If the computer simulation had been started with an (undisturbed) roll pattern of $\bar{k}<k_c$ (e.g., 24 rolls instead of 27) an analogous scenario would have happened near the entrance of the cell at the lower Eckhaus boundary $k_E^-=k_c-[\epsilon/(3\xi_0^2)]^{1/2}$. The stability condition for stationary deformed patterns, therefore, reads

$$\left.\begin{matrix}k_{\max}\\k_{\min}\end{matrix}\right\}\equiv k\left[x=\left\{\begin{matrix}\Gamma\\0\end{matrix}\right\}\right]$$
$$=k_c+q\pm\frac{\Gamma}{2}\frac{\omega_c+\Omega}{D_\parallel}\lesseqgtr k_c\pm[\epsilon/(3\xi_0^2)]^{1/2}\equiv\left\{\begin{matrix}k_E^+\\k_E^-\end{matrix}\right., \tag{5.20a}$$

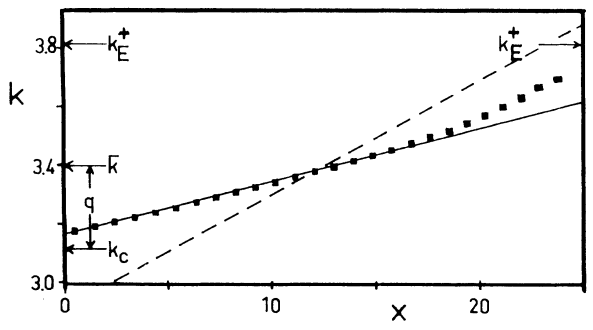

FIG. 9. Wave-number distribution (solid squares) resulting at Re=0.0083 from an initial pattern of 27 rolls at Re=0 under phase-pinning BC. The solid line represents the corresponding solution of the phase equation (5.19). Near outlet $k(x)$ almost reaches the upper Eckhaus boundary k_E^+. After increasing the flow rate to Re=0.0167 the Eckhaus threshold is crossed at the outlet, the system becomes locally unstable there, and a pair of rolls is annihilated (see Fig. 10). The dashed line denotes the stationary solution (5.19) that is for Re=0.0167 Eckhaus unstable at k_E^+. The lower Eckhaus threshold k_E^- is well below the k window shown.

or equivalently

$$(\omega_c+\Omega)<\frac{2}{\Gamma}D_\parallel\{[\epsilon/(3\xi_0^2)]^{1/2}-|q|\}\ . \tag{5.20b}$$

The different parameters entering into (5.20) are the flow rate Re via $\omega_c+\Omega$, the Rayleigh number Ra via ϵ, the wave number of the basic undisturbed structure via q, and the channel length Γ. For the present computer simulation with $q=0.277$, $\Gamma=25$, and $\epsilon=0.215$ Eq. (5.20b) predicts a critical Reynolds number of $\mathrm{Re}_1=0.014$. Figure 10 shows the time evolution of the lateral positions of the roll centers after increasing the flow rate, beyond this value to Re=0.0167. The local Eckhaus instability occurring near the outlet annihilates two convective rolls there, so that the average wave number shrinks to $\bar{k}'=25\pi/\Gamma=\pi$. The resulting new k distribution being shifted downwards by $\bar{k}-\bar{k}'=2\pi/\Gamma$ lies completely within the stable Eckhaus band. Thus by annihilation of two convection rolls the pattern has restabilized. According to (5.20) the critical flow rate for this new stable 25-roll state (with $q'=\bar{k}'-k_c=0.025$) is $\mathrm{Re}_2=0.028$. Since the new wave-number profile $\bar{k}'(x)$ is practically concentric with the Eckhaus band a further increase of Re beyond Re_2 causes k_E^+ and k_E^- to be crossed *simultaneously*. That causes *repeated* roll creation near the inlet and roll annihilation near the outlet and a *traveling* pattern in the bulk of the channel as shown in Fig. 11.

By imposing $q=0$ in (5.20b) we obtain an estimate for the critical flow rate for the onset of roll propagation

$$\mathrm{Re}\simeq\frac{2.126}{\sigma+0.3432}\frac{\sqrt{\epsilon}}{\Gamma}\ . \tag{5.21}$$

Here we used $\xi_0^2=0.148$ and $\tau_0=(\sigma+0.5117)/19.65\sigma$. This is only an upper limit for the transition because the nonlinearities of the wave-number distribution $k(x)$ are not taken into account.

Finally we give some reasoning why the phase equation of Pocheau *et al.* [26]

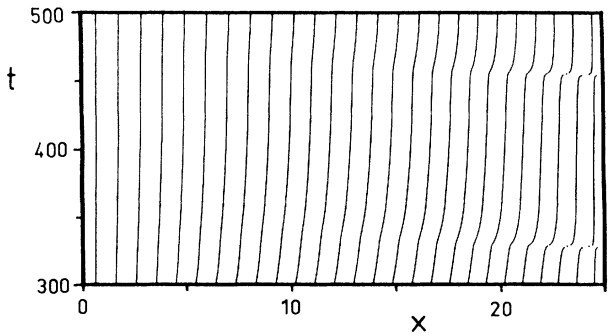

FIG. 10. Time evolution of the nodes of the vertical velocity field $w(x,z=0.5,t)$ after the flow rate has been stepped up to Re=0.0167. Since the stationary wave-number distribution (5.19) is for $q=0.277$, $\Gamma=25$, $\epsilon=0.215$, and Re=0.0167 locally Eckhaus unstable two convection rolls are annihilated (at $t\simeq320$ and $\simeq460$) and a new stationary pattern of 25 rolls stabilizes. The averaged wave number, therefore, reduces to the new value $\bar{k}'=25\pi/25=\pi$.

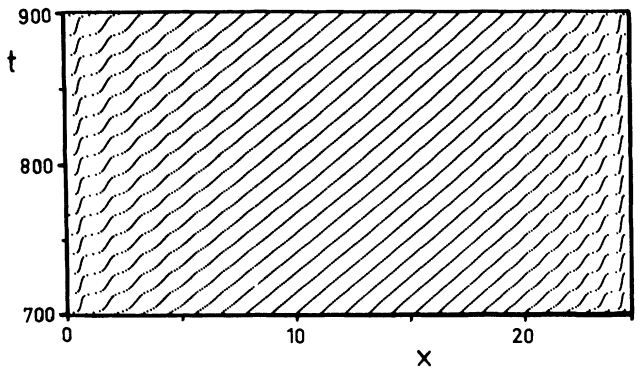

FIG. 11. Time evolution of the nodes of the vertical velocity field $w(x,z=0.5,t)$ under phase-pinning BC. For these parameters ($\epsilon=0.215$, Re=0.0833) a stationary pattern is Eckhaus unstable both at inlet and outlet according to (5.21). Creation and annihilation of rolls at inlet and outlet, respectively, and downstream pattern propagation in the bulk occurs.

$$\partial_t\varphi=D_{\parallel}\partial_x^2\varphi-U\partial_x\varphi \tag{5.22}$$

leads to the same results as our inhomogeneous equation (5.15): The quantities φ and ψ are related by $\varphi=k_c x+\psi$ and U is the momentary propagation speed of the pattern when a throughflow is suddenly switched on. Substitution into (5.22) and neglecting terms of order Re^2 gives

$$\partial_t\psi=D_{\parallel}\partial_x^2\psi-U(k_c+q)\ . \tag{5.23}$$

Since an undisturbed roll pattern subjected to a sudden throughflow is not immediately affected by the presence of (phase pinning) lateral boundaries it is reasonable to identify the momentary velocity U with the propagation speed of the pattern if there were no phase pinning,

$$U=v_{\text{phase}}\equiv\frac{\omega_c+\Omega}{k_c+q}\ . \tag{5.24}$$

By inserting (5.24) into (5.23) we recover our inhomogeneous phase equation (5.15).

VI. SUMMARY

We have investigated the Rayleigh-Bénard problem subjected to a plane Poiseuille shear flow perpendicular to the roll chain. This convective structure can be realized experimentally in a long narrow conduit if a weak throughflow is imposed. Although channel sidewalls are essential for transversal rolls to appear, we used for the sake of mathematical simplicity a two-dimensional description for the fields in a vertical plane perpendicular to the roll axes. Results obtained by an amplitude equation are presented and compared with computer simulations of the full 2D hydrodynamic field equations. The main issue of our analysis is the influence of different inlet and outlet boundary conditions on the nonlinear convective structure.

The most simple BC's are periodic ones appropriate to simulate a channel of infinite length. For supercritical drive, $\epsilon>\epsilon_c$, the whole duct is filled with convection rolls traveling downstream. Vertical heat transport as well as pattern propagation velocity observed in the simulations agree well with the solution of the amplitude equation. The latter also yields the theoretical explanation for the phase velocity to decrease with growing Rayleigh number.

Convection patterns with space-dependent envelopes appear if more realistic BC's are imposed: If convective motion is suppressed at the cell apertures a more or less extended region near the inlet of the channel remains free of convection whereas the remaining part of the duct is filled with traveling rolls. Within this bulk region the wavelength of the structure is uniquely selected by the final control parameter combination independent of the geometry and history of the system. Increasing the flow rate broadens the conductive region to the debit of the convective one. If a critical Reynolds number is exceeded any convection is "blown" out of the duct even though the basic conductive state is unstable. This is because the system has become convectively unstable and *initial* perturbations are carried out of the cell. At the same time the system becomes very sensitive against *permanent* perturbations: If such a continuous source of noise (e.g., inlet turbulence, perturbations, thermal noise) is present, the disturbances are amplified exponentially downstream and generate "noise-sustained" convective structures with fluctuating phase. These states disappear as soon as the noise is removed. On the other hand, if the system is absolutely unstable noise does not play an important role because the occurring convection is not appreciably affected by small perturbations.

Motivated by experiments of Pocheau *et al.* [26], we also have considered BC's pinning the phase of the convective rolls at the cell apertures. The standing deformed patterns, which appear for small flow rates, are explained by an inhomogeneous phase equation obtained by a Reynolds number expansion of the amplitude equation. It could be shown that this phase equation is equivalent to the one discussed earlier [26]. For increasing throughflow the deformed structure becomes unstable due to a local Eckhaus instability. Roll generation or annihilation occurs resulting finally in a transition to traveling rolls.

ACKNOWLEDGMENTS

Discussions with G. Ahlers, K. L. Babcock, E. Bodenschatz, S. Trainoff, and M. Tveitereid are gratefully acknowledged. This work was supported by Volkswagen-Stiftung.

APPENDIX A: EXPANSION OF ω_c, Ra_c, AND v_g FOR SMALL THROUGHFLOW RATES

For a convection channel of infinite length it is convenient to expand the x dependences of w and θ in plane waves. At the threshold Ra_c there is only the critical

mode excited:

$$\begin{bmatrix} w(x,z,t) \\ \theta(x,z,t) \end{bmatrix} = \begin{bmatrix} \hat{w}(z) \\ \hat{\theta}(z) \end{bmatrix} e^{i(k_c x-\omega_c t)} + \text{c.c.} \tag{A1}$$

where $k_c = k_c(\mathrm{Re})$ denotes the critical wave number in the presence of throughflow. Inserting (A1) into (2.1) and dropping the nonlinear terms leads to the linear stability problem:

$$\begin{bmatrix} i\omega_c(\partial_z^2-k_c^2)+\sigma(\partial_z^2-k_c^2)^2-6ik_c\sigma\,\mathrm{Re}[2+z(1-z)(\partial_z^2-k_c^2)] & -\sigma k_c^2 \\ \mathrm{Ra}_c & i\omega_c+(\partial_z^2-k_c^2)-6ik_c\sigma\,\mathrm{Re}z(1-z) \end{bmatrix} \begin{bmatrix} \hat{w}(z) \\ \hat{\theta}(z) \end{bmatrix} = 0 \tag{A2}$$

with the boundary conditions

$$\hat{w} = \partial_z \hat{w} = \hat{\theta} = 0 \quad \text{at } z=0 \text{ and } z=1 \,. \tag{A3}$$

This problem is only solvable for special values of $\mathrm{Ra}_c(\mathrm{Re})$ and $\omega_c(\mathrm{Re})$. Accordingly we expand for small Re:

$$\begin{aligned} \begin{bmatrix} \hat{w}(z) \\ \hat{\theta}(z) \end{bmatrix} &= \begin{bmatrix} \hat{w}_0(z) \\ \hat{\theta}_0(z) \end{bmatrix} + i \begin{bmatrix} \hat{w}_1(z) \\ \hat{\theta}_1(z) \end{bmatrix} \mathrm{Re} \\ &\quad + \begin{bmatrix} \hat{w}_2(z) \\ \hat{\theta}_2(z) \end{bmatrix} \mathrm{Re}^2 + O(\mathrm{Re}^3) \,, \\ \mathrm{Ra}_c &= \mathrm{Ra}_c^0 + \mathrm{Ra}_2 \mathrm{Re}^2 + O(\mathrm{Re}^4) \,, \\ \omega_c &= \omega_1 \mathrm{Re} + O(\mathrm{Re}^3) \,, \end{aligned} \tag{A4}$$

where the symmetry conditions for Ra_c and ω_c (Ra_c even, ω_c odd in Re) have already been taken into account. Inserting (A4) into (A2) leads to a hierarchic system of inhomogeneous boundary value problems for $\hat{w}_i(z)$, $\hat{\theta}_i(z)$, which all have to fulfill (A3). In lowest expansion order (Re=0) Eq. (A2) yields the Rayleigh-Bénard stability problem

$$\begin{bmatrix} (\partial_z^2-k_c^2)^2 & -k_c^2 \\ \mathrm{Ra}_c^0 & \partial_z^2-k_c^2 \end{bmatrix} \begin{bmatrix} \hat{w}_0 \\ \hat{\theta}_0 \end{bmatrix} = 0 \,, \tag{A5}$$

where $\mathrm{Ra}_c^0 = 1707.76$ is the critical Rayleigh number without flow. The adjoint solution

$$\begin{bmatrix} \hat{w}_0^\dagger \\ \hat{\theta}_0^\dagger \end{bmatrix} = \begin{bmatrix} \mathrm{Ra}_c^0 \hat{w}_0 \\ -k_c^2 \hat{\theta}_0 \end{bmatrix} \tag{A6}$$

is necessary to formulate the solvability conditions in the next expansion orders. In $O(\mathrm{Re}^1)$ one obtains from (A2) the following system for $\hat{w}_1(z)$ and $\hat{\theta}_1(z)$:

$$\begin{aligned} &\begin{bmatrix} (\partial_z^2-k_c^2)^2 & -k_c^2 \\ \mathrm{Ra}_c^0 & \partial_z^2-k_c^2 \end{bmatrix} \begin{bmatrix} \hat{w}_1 \\ \hat{\theta}_1 \end{bmatrix} \\ &\quad = \begin{bmatrix} k_c \left[12 + \left[6z(1-z) - \dfrac{\omega_1}{\sigma k_c} \right] (\partial_z^2-k_c^2) \hat{w}_0 \right] \\ \sigma k_c \left[6z(1-z) - \dfrac{\omega_1}{\sigma k_c} \right] \hat{\theta}_0 \end{bmatrix} . \end{aligned} \tag{A7}$$

The requirement that the inhomogeneity on the right-hand side of (A7) has to be orthogonal to the adjoint solution (A6) yields the coefficient

$$\omega_1 = \sigma k_c \frac{\langle \hat{w}_0^\dagger | [12+6z(1-z)(\partial_z^2-k_c^2)] \hat{w}_0 \rangle + \sigma \langle \hat{\theta}_0^\dagger | 6z(1-z)\hat{\theta}_0 \rangle}{\langle \hat{w}_0^\dagger | (\partial_z^2-k_c^2)\hat{w}_0 \rangle + \sigma \langle \hat{\theta}_0^\dagger | \hat{\theta}_0 \rangle} \,. \tag{A8}$$

The brackets abbreviate integration between $z=0$ and 1. Analogously the solvability condition in $O(\mathrm{Re}^2)$ gives the expansion coefficient

$$\mathrm{Ra}_2 = -k_c \frac{\left\langle \hat{w}_0^\dagger \middle| \left[12 + \left[6z(1-z) - \dfrac{\omega_1}{\sigma k_c} \right] (\partial_z^2-k_c^2) \right] \hat{w}_1 \right\rangle + \sigma \left\langle \hat{\theta}_0^\dagger \middle| \left[6z(1-z) - \dfrac{\omega_1}{\sigma k_c} \right] \hat{\theta}_1 \right\rangle}{\langle \hat{\theta}_0^\dagger | \hat{w}_0 \rangle} \,. \tag{A9}$$

By virtue of (A8) and (A9) and taking into account that the functions $\hat{w}_1$ and $\hat{\theta}_1$ in Ra_2 are also σ dependent the structural σ dependences of ω_c and Ra_c are found to be of the form

$$\omega_c = \sigma \frac{a_0+a_1\sigma}{a_2+a_3\sigma} \mathrm{Re} + O(\mathrm{Re}^3) \,, \tag{A10}$$

$$\mathrm{Ra}_c = \mathrm{Ra}_c^0 + \frac{b_0+b_1\sigma+b_2\sigma^2+b_3\sigma^3+b_4\sigma^4}{(a_2+a_3\sigma)^2} \mathrm{Re}^2 + O(\mathrm{Re}^4) \,. \tag{A11}$$

The factors a_i, b_i can be calculated either by successive solution of the boundary value problems (A5), (A7), and

evaluation of the integrals or—more conveniently if a computer solution of the stability problem is available—by fitting them to the exact numerical results for different Prandtl numbers σ. The results of the latter procedure are given by Eqs. (3.1) and (3.2). The same procedure has been applied to derive an expression for the group velocity $v_g=\partial\omega_c/\partial k_c$, presented by Eq. (4.3).

APPENDIX B: DERIVATION OF THE AMPLITUDE EQUATION

To determine the *linear* coefficients τ_0, v_g, ξ_0^2, c_0, and c_1 the right-hand side of Eq. (2.3) is set equal to zero and the x dependence of the solution is expanded into planes waves proportional to e^{ikx}. For given Ra, k, Re, and σ the solution can be written in the form

$$\begin{bmatrix} w(x,z,t) \\ \theta(x,z,t) \end{bmatrix} = \begin{bmatrix} \hat{w}(z) \\ \hat{\theta}(z) \end{bmatrix} e^{ikx+st} + \text{c.c.}$$

where the complex growth exponent $s=\nu-i\omega$, as well as the z dependences $\hat{w}(z)$ and $\hat{\theta}(z)$ are to be calculated numerically (e.g., by a shooting algorithm). The linear coefficients then arise [30] by evaluating the following derivatives at the critical point k_c,Ra_c:

$$\tau_0=\frac{1}{\mathrm{Ra}(\partial\nu/\partial\,\mathrm{Ra})}\bigg|_c,\quad c_0=-\mathrm{Ra}\tau_0\frac{\partial\omega}{\partial\,\mathrm{Ra}}\bigg|_c,\quad v_g=\frac{\partial\omega}{\partial k}\bigg|_c$$

$$\xi_0^2=\frac{1}{2\,\mathrm{Ra}}\frac{\partial^2\mathrm{Ra}}{\partial k^2}\bigg|_c,\quad c_1=\frac{\tau_0}{2\xi_0^2}\frac{\partial^2\omega}{\partial k^2}\bigg|_c .$$

In order to derive the *nonlinear* coefficients γ and c_2, the nonlinear equation (2.3) is needed and we abbreviate it in the form

$$\mathcal{L}Y=N . \tag{B1}$$

Writing $\mathrm{Ra}=\mathrm{Ra}_c(\sigma,\mathrm{Re})(1+\mu)$ we expand $\mathcal{L}$, Y, and N in powers of $\mu^{1/2}$. Since the spatial translation symmetry of the system forbids nonlinear derivative terms in the amplitude equation to appear up to the considered expansion order $\mu^{3/2}$ it is not necessary to introduce slow time and space scales. We therefore get

$$\begin{aligned} &\mathcal{L}=\mathcal{L}_0+\mu\mathcal{L}_2 , \\ &Y=\mu^{1/2}A_0Y_1+\mu Y_2+\mu^{3/2}Y_3+\cdots , \\ &N=\mu N_2+\mu^{3/2}N_3+\cdots , \end{aligned} \tag{B2}$$

where $\mu^{1/2}A_0=A$ is the amplitude of the lowest-order solution Y_1. Equation (B1) then splits into a hierarchic system of *linear* inhomogeneous boundary value problems for the Y_i:

$$A_0\mathcal{L}_0Y_1=0 \quad \text{for } O(\mu^{1/2}) , \tag{B3a}$$

$$\mathcal{L}_0Y_2=N_2 \quad \text{for } O(\mu) , \tag{B3b}$$

$$\mathcal{L}_0Y_3=-A_0\mathcal{L}_2Y_1+N_3 \quad \text{for } O(\mu^{3/2}) . \tag{B3c}$$

This system is only solvable if certain conditions are fulfilled. These solvability conditions yield a nonlinear equation for A_0 which contains the coefficients γ and c_2. In the following we give some details of the procedure to solve (B3).

Equation (B3a) defines the linear stability problem with the eigensolution

$$Y_1=\begin{bmatrix} \hat{w}(z) \\ \hat{\theta}(z) \end{bmatrix} e^{i(k_cx-\omega_ct)}+\text{c.c.} \tag{B4}$$

at onset $\mathrm{Ra}=\mathrm{Ra}_c(\sigma,\mathrm{Re})$. Equation (B3b) is only solvable if the scalar product of the inhomogeneity N_2 with the adjoint solution $Y_1^\dagger$ vanishes:

$$\langle Y_1^\dagger|N_2\rangle=0 . \tag{B5}$$

Here the bracket denotes integration over the whole fluid layer. The condition (B5) is trivially fulfilled since the (quadratic) nonlinearity N_2 with its x dependencies $e^{\pm 2ik_cx}$ and $e^0=1$ is out of resonance with the adjoint solution $Y_1^\dagger\propto e^{i(k_cx-\omega_ct)}$. The solution Y_2 separates in the form

$$Y_2=|A_0|^2\hat{\psi}_0(z)+A_0^2\hat{\psi}_2(z)e^{2i(k_cx-\omega_ct)}+\text{c.c.} \tag{B6}$$

where the $\hat{\psi}_i(z)$ are z dependencies to be calculated. The quadratic nonlinearity in (B3c) couples Y_1 with Y_2 so that N_3 is of the form

$$N_3=|A_0|^2A_0\hat{\chi}_1(z)e^{i(k_cx-\omega_ct)}+\cdots \tag{B7}$$

where the ellipsis represents nonresonant terms, which are unimportant for the following discussion since their scalar product with $Y_1^\dagger$ drops out. Consequently the solvability condition in $O(\mu^{3/2})$ reads

$$0=\langle Y_1^\dagger|\mathcal{L}_2Y_1\rangle A_0-\langle Y_1^\dagger|\hat{\chi}_1(z)e^{i(k_cx-\omega_ct)}\rangle|A_0|^2A_0 , \tag{B8}$$

where the brackets denote numbers to be evaluated numerically. Note that we treat here the special situation where A_0 depends neither on time nor space. The coefficients γ and c_2 arise by comparison of (B8) with the space- and time-independent amplitude equation (4.1). One obtains

$$1+ic_0=\langle Y_1^\dagger|\mathcal{L}_2Y_1\rangle , \tag{B9a}$$

$$\gamma(1+ic_2)=\langle Y_1^\dagger|\hat{\chi}_1(z)e^{i(k_cx-\omega_ct)}\rangle . \tag{B9b}$$

All coefficients of the amplitude equation depend on the throughflow rate Re as well as the Prandtl number σ. The following fit formulas give the leading Re dependencies for $\sigma=1$:

$$\begin{aligned} &\tau_0\simeq 7.693\times10^{-2}\left[1-\left[\frac{\mathrm{Re}}{39.13}\right]^2\right],\quad c_0\simeq\frac{\mathrm{Re}}{140.1} , \\ &\xi_0^2\simeq 0.148\left[1-\left[\frac{\mathrm{Re}}{35.24}\right]^2\right],\quad c_1\simeq\frac{\mathrm{Re}}{39.98} , \\ &v_g\simeq 1.229\,\mathrm{Re} , \\ &\gamma\simeq 0.7027\left[1-\left[\frac{\mathrm{Re}}{332.6}\right]^2\right],\quad c_2\simeq\frac{\mathrm{Re}}{387} . \end{aligned} \tag{B10}$$

The expressions for c_1, γ, and c_2 given earlier [20] differ slightly from (B10); they are not correct.

[1] For a review see R. E. Kelly, in *The Onset and Development of Rayleigh-Bénard Convection in Shear Flows,* Proceedings of the International Conference on Physical Chemistry and Hydrodynamics, 1977, edited by D. B. Spaulding (London, 1977), p. 65.
[2] See references in Ref. 12.
[3] S. Chandrasekhar, *Hydrodynamic and Hydromagnetic Stability* (Oxford University Press, New York, 1981).
[4] J. K. Platten and J. C. Legros, *Convection in Liquids* (Springer, Berlin, 1984).
[5] H. Bénard and D. Avsec, J. Phys. Radium **9**, 486 (1938).
[6] D. Brunt, *Compendium of Meteorology* (American Meteorological Society, Boston, 1951), p. 1255.
[7] J. M. Luijkx, Ph.D. thesis, University of Mons (Belgium), 1983.
[8] Y. Mori and Y. Uchida, Int. J. Heat Mass Transfer **9**, 803 (1966).
[9] Y. Kamotani and S. Ostrach, J. Heat Transfer **98**, 62 (1976).
[10] G. J. Hwang and C. L. Liu, Can. J. Chem. Eng. **54**, 521 (1976).
[11] J. M. Luijkx, J. K. Platten, and J. C. Legros, Int. J. Heat Mass Transfer **24**, 1287 (1981).
[12] K. C. Chiu and F. Rosenberger, Int. J. Heat Mass Transfer **30**, 1645 (1987).
[13] M. T. Ouazzani, J. K. Platten, and A. Mojtabi, Int. J. Heat Mass Transfer **33**, 1417 (1990).
[14] Y. Ogura and A. Yagihashi, J. Meteorol. Soc. Jpn. **47**, 205 (1969).
[15] G. J. Hwang and K. C. Cheng (unpublished).
[16] F. B. Lipps, J. Atmos. Sci. **28**, 3 (1971).
[17] K. Fukui and M. Nakajima, Int. J. Heat Mass Transfer **26**, 109 (1983).
[18] M. T. Ouazzani, J. P. Caltagirone, G. Meyer, and A. Mojtabi, Int. J. Heat Mass Transfer **32**, 261 (1989).
[19] G. Evans and R. Greif, Int. J. Heat Mass Transfer **32**, 895 (1989).
[20] H. W. Müller, M. Lücke, and M. Kamps, Europhys. Lett. **10**, 451 (1989); in *Ordered and Turbulent Patterns in Taylor-Couette Flow, NATO Advanced Study Institute, Series B: Physics,* edited by C. D. Andereck and F. Hayot (Plenum, New York, in press).
[21] A. Tsameret and V. Steinberg, Europhys. Lett. **14**, 331 (1991); Phys. Rev. Lett. **67**, 3392 (1991).
[22] K. L. Babcock, G. Ahlers, and D. S. Cannell, Phys. Rev. Lett. **67**, 3388 (1991).
[23] M. T. Ouazzani, J. K. Platten, and A. Mojtabi (unpublished).
[24] H. R. Brand, G. Ahlers, and R. J. Deissler, Phys. Rev. A **43**, 4262 (1991).
[25] H. W. Müller, S. Trainoff, and M. Tveitereid (unpublished).
[26] A. Pocheau, V. Croquette, P. Le Gal, and C. Poitou, Europhys. Lett. **3**, 915 (1987).
[27] K. S. Gage and W. H. Reid, J. Fluid Mech. **33**, 21 (1968).
[28] S. H. Davis, J. Fluid Mech. **30**, 465 (1967).
[29] K. Stork and U. Müller, J. Fluid Mech. **54**, 599 (1972).
[30] A. C. Newell, Lect. Appl. Math. **15**, 157 (1974).
[31] P. Huerre, in *Propagation in Systems Far from Equilibrium,* edited by J. E. Wesfreid, H. R. Brand, P. Manneville, G. Albinet, and N. Boccara (Springer, Berlin, 1988), p. 340.
[32] M. C. Cross, Phys. Fluids **23**, 1727 (1980).
[33] G. Dee and J. S. Langer, Phys. Rev. Lett. **50**, 383 (1983).
[34] J. E. Welch, F. H. Harlow, J. P. Shannon, and B. J. Daly, Los Alamos Scientific Laboratory Report No. LA-3425, 1966 (unpublished).
[35] M. Lücke, M. Mihelcic, B. Kowalski, and K. Wingerath, in *The Physics of Structure Formation: Theory and Simulation,* edited by W. Güttinger and G. Dangelmayr (Springer, Berlin, 1987).
[36] C. W. Hirt, B. D. Nichols, and N. C. Romero, Los Alamos Scientific Laboratory Report No. LA-5652, 1975 (unpublished).
[37] M. T. Ouazzani and J. K. Platten (private communication).
[38] R. J. Deissler, Physica D **25**, 233 (1987).
[39] H. R. Brand, Phys. Rev. A **35**, 4461 (1987).